Enhanced cryogenic thermopower in $SrTiO_3$ by ionic gating

Sunao Shimizu,[1,*] Shimpei Ono,[2] Takafumi Hatano,[3] Yoshihiro Iwasa,[1,4] and Yoshinori Tokura[1,4]
[1]*RIKEN Center for Emergent Matter Science (CEMS), Wako, Saitama 351-0198, Japan*
[2]*Central Research Institute of Electric Power Industry, Material Science Research Laboratory, Yokosuka, Kanagawa 240-0196, Japan*
[3]*Department of Crystalline Materials Science, Nagoya University, Chikusa, Nagoya 464-8603, Japan*
[4]*Quantum Phase Electronics Center and Department of Applied Physics, University of Tokyo, Bunkyo, Tokyo 113-8656, Japan*
(Received 26 May 2015; published 2 October 2015)

Ion-gated transistors have enabled us to electrically control electronic phase transitions such as superconductivity in a variety of materials. On the other hand, the carrier doping mechanism, particularly in oxide semiconductors, still remains elusive. Here, we report on the low-temperature thermopower of two-dimensional electron systems in ion-gated $SrTiO_3$. We found that the metallic states induced by ionic gating exhibit a large peak in thermoelectric power to over 1 mV/K at around 20 K. This enhancement of cryogenic thermoelectric power is ascribed to a phonon-drag effect, which is in general dramatically suppressed by conventional chemical doping because the phonon mean free path is suppressed by chemical disorder. The large sustained peak, even in the high carrier density regime of 2×10^{14} cm^{-2}, strongly indicates that a less disordered process, i.e., electrostatic charge accumulation, dominates over electrochemical carrier doping in the ionic gating in $SrTiO_3$.

DOI: 10.1103/PhysRevB.92.165304 PACS number(s): 73.40.−c, 73.50.Lw

I. INTRODUCTION

Ion-gated transistors, which we employed in this study, attract much attention because of their ability to tune carrier densities in the order of 10^{14} cm^{-2} and the consequent electric phase control, including the gate-induced insulator-metal transition [1,2], ferromagnetism [3], and also superconductivity [4–7]. Despite such successful manipulations of novel interface phenomena in a wide spectrum of material systems, the mechanism of ionic gating is still controversial. If we focus on oxide-based ion-gated transistors, possible mechanisms are discussed mainly in two directions. One explanation is the electrostatic mechanism, in which the charges are accumulated in electric double layers that work as nanogap capacitors [4]. The other is the electrochemical reaction, in which reversible creation and annihilation of oxygen vacancies occur near the material surface due to the large electric field at the electric double layer [8].

We focused on the Seebeck effect, which reflects not only the electronic band structure but also the coupling of the charge transport carriers with phonons. Especially, when the Seebeck coefficient S (or thermopower) shows a large enhancement in a cryogenic temperature region due to the phonon-drag effect [9], the peak height can be a measure of disorder in the crystal structures. It is known that the peak height of the low-temperature thermopower is proportional to the phonon mean free path λ, which depends strongly on the dopant or defect density in crystals [10,11]. For instance, the phonon-drag effect is weakened very rapidly by proceeding element substitutions necessary for chemical carrier doping [11]. This means that in oxide-based ion-gated transistors, the evaluation of the phonon-drag thermopower is a touchstone issue for the proposed doping mechanisms: the electrostatic field effect and electrochemical reaction. More importantly, if electrostatic carrier doping is dominating in the ionic gating, the extremely large thermopower is anticipated concomitantly with high electrical conductivity. This would lead to a large thermoelectric power factor in a cryogenic region, which is required for novel thermoenergy device applications such as thermoelectric cooling [12,13].

In this paper, we report on the gate tuning of transport and thermoelectric properties in an oxide semiconductor, $SrTiO_3$, which is a thermoelectric material that has been investigated extensively for decades [11,14–17]. The basic thermoelectric properties of doped (or reduced) single crystals [11,14–17] and thin films [11] are already well known, making $SrTiO_3$ the best choice to investigate the effect of ionic gating on thermoelectric properties.

II. EXPERIMENT

Electric-double-layer transistor configurations were employed for the gating experiments, where single crystalline $SrTiO_3$ and InP were used as channel materials. Figure 1(a) shows a schematic diagram illustrating the gate-induced metallic layer in $SrTiO_3$. The application of a gate voltage V_G to a gate electrode induces redistribution of ions in the gel, resulting in the formation of the electric double layer with charge accumulated on the surface of $SrTiO_3$. Figures 1(b) and 1(c) illustrate the ion-gated transistors prepared for this study; the configuration in Fig. 1(b) was used for the device characterization in Secs. III A and III B, and the configuration in Fig. 1(c) was used for the thermoelectric measurements in Secs. III C and III D. We performed all the experiments in a vacuum condition with a chamber pressure of $\sim10^{-5}$ Torr in order to avoid the impact of gas molecules on the ion-gated devices [8,18].

The $SrTiO_3$-based devices were fabricated on an atomically flat (100) surface. Ti/Au electrodes with thicknesses of 5/50 nm were evaporated to form drain and source electrodes. The surface just beneath the electrodes was metallized by ion milling [19] to make Ohmic contacts. An ion-gel sheet was used as a gate dielectric, which was prepared in a conventional

*sshimizu@riken.jp

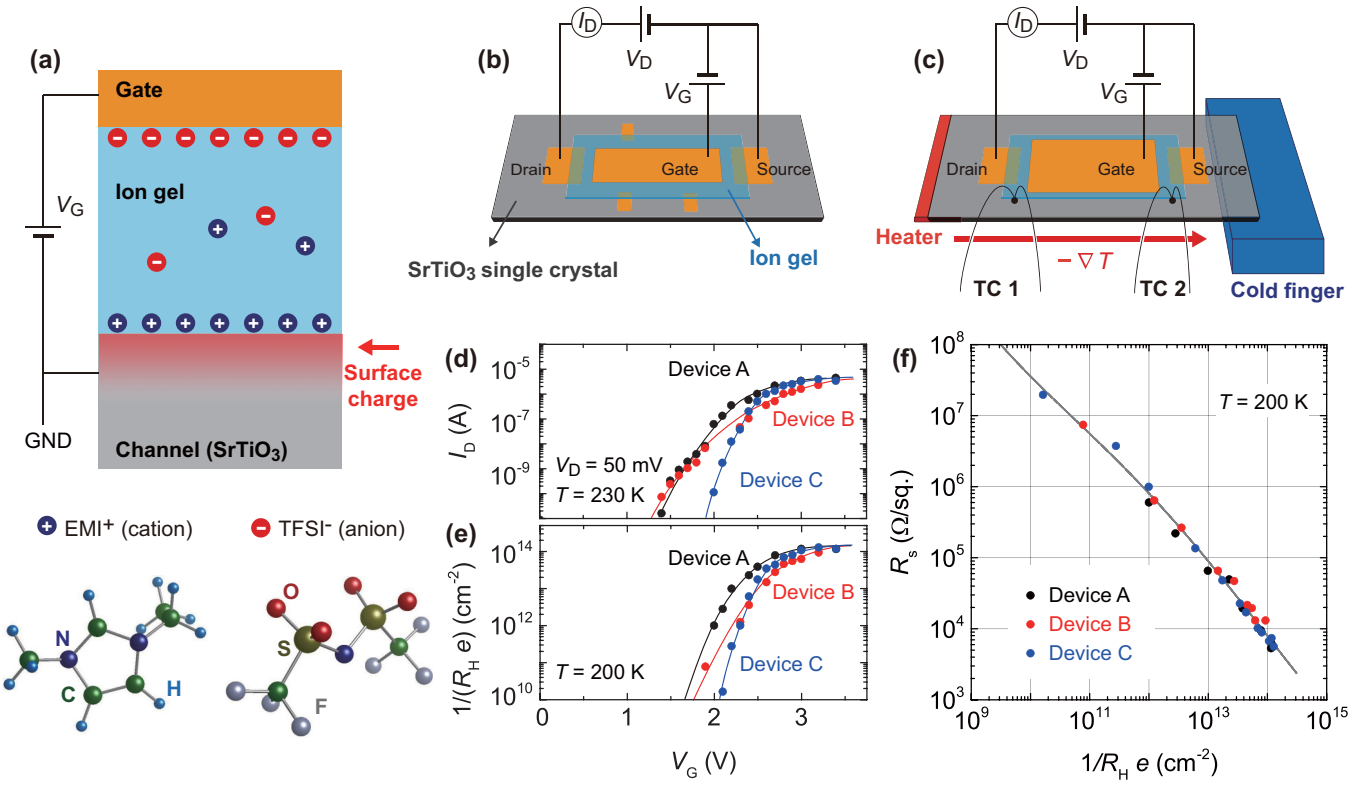

FIG. 1. (Color online) Schematic structures and transfer characteristics of $SrTiO_3$-based ion-gated transistors. (a) Formation of the gate-induced metallic conduction layer at the electric double-layer interface. When a positive gate bias V_G is applied to the gate electrode, ions in the ion gel redistribute and form the electric double layer with a surface charge accumulated on the surface of $SrTiO_3$. Lower figures show the chemical structures of 1-ethyl-3-methylimidazolium cation, EMI+, and bis(trifluoromethylsulfonyl)imide anion, TFSI−. EMI-TFSI is used as conducting ionic liquid in the gel dielectric. (b) Schematic diagram of device structure with Hall bar geometry. (c) Schematic diagram of a setup used for Seebeck effect measurements. The resistance and the Seebeck coefficient are simultaneously measured in this setup. Here, V_D, I_D, and TC stand for the source-drain voltage, current, and thermocouple, respectively. (d) Transfer characteristics for devices A, B, and C obtained with configuration in (b). The values of I_D show a sharp rise at $V_G \sim 2$ V and saturate at $V_G \sim 3.5$ V. (e) V_G dependence of sheet carrier density, $N = 1/(R_H e)$, for devices A, B, and C. The values of N exceed 1×10^{14} cm^{-2} at $V_G \sim 3$ V. (f) Plots of sheet resistance R_s vs N at 200 K. The data for the three devices fall on a universal curve. The solid line is a fitting curve for log R_s with a fourth-order polynomial of log N.

way [20,21]. The gel dielectric was cut and put on the $SrTiO_3$ surface, bridging the drain and source electrodes, as shown in Figs. 1(b) and 1(c). The ion gel contained the following cation and anion: 1-ethyl-3-methylimidazolium (EMI+) and bis(trifluoromethylsulfonyl)imide (TFSI−). The chemical structures of those ions are shown on the bottom of Fig. 1(a). The typical sizes of the $SrTiO_3$ single crystal, the drain (source) electrode, and the ion-gel sheet were 5 mm × 3 mm, 0.6 mm × 0.7 mm, and 2 mm × 1.5 mm, respectively. The InP-based device has a similar structure and was fabricated on a semi-insulating InP (111) substrate.

For the thermoelectric measurements, a heater was attached on one end of the device, as shown schematically in Fig. 1(c), and it produced a thermal gradient $-\nabla T$ from the heater to the cold finger. This configuration allowed us to measure the sheet resistance R_s and S simultaneously, as reported elsewhere [22]. The values of S were estimated by measuring the temperature difference ΔT (0 to 1 K) and the thermal voltage ΔV between the drain and source electrodes. Two thermocouples [TC 1 and TC 2 in Fig. 1(c)] were attached to monitor ΔT at both edges of the channel. The values of S were evaluated from the slope of the ΔV-ΔT plots.

III. RESULTS

A. Tunability of conduction electrons in ion-gated $SrTiO_3$

As mentioned above, a large amount of charge carriers can be accumulated in the electric double layer under a gate electric field. To evaluate the tunability of the carrier density in our ion-gated $SrTiO_3$, we prepared three devices (devices A, B, and C) with the Hall bar configuration shown in Fig. 1(b). Figure 1(d) shows the transfer characteristics of the three devices at 230 K when the drain-source bias V_D was 50 mV. All devices showed a sharp increase in the drain-source current I_D at $V_G \sim 2$ V and saturation at $V_G \sim 3.5$ V. The sheet carrier density N, which is estimated from the Hall coefficient R_H and the elementary charge e as $1/(R_H e)$, is shown in Fig. 1(e). The maximum value obtained here is 1×10^{14} to 2×10^{14} cm^{-2}, which is comparable with previous reports on $SrTiO_3$-based ion-gated devices [4,23]. Note here that the plots for R_s versus $1/(R_H e)$ at 200 K fall on a universal curve over a wide range of four decades both in R_s and $1/(R_H e)$, as shown in Fig. 1(f). The experimental relationship between R_s and N [$=1/(R_H e)$] allows us to estimate N for other ion-gated $SrTiO_3$ devices by using the R_s values below.

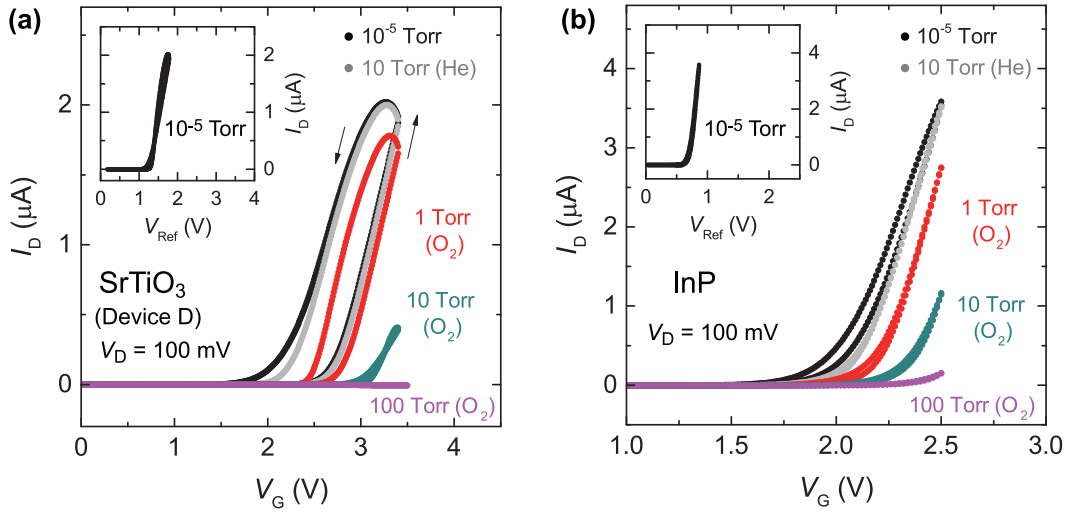

FIG. 2. (Color online) Transfer characteristics of ion-gated devices in an O_2-gas atmosphere. (a) Transfer characteristics of ion-gated $SrTiO_3$ at room temperature. In a high vacuum ($\sim 10^{-5}$ Torr) and He gas atmosphere (10 Torr), typical n-type transistor operations are observed. In an O_2 gas atmosphere, however, the drain-source current I_D was dramatically suppressed. The inset plots I_D against the reference voltage V_{Ref}. The hysteresis in I_D-V_{Ref} characteristics is very tiny, suggesting that the hysteresis in I_D-V_G (the gate voltage) originates from the slow reformation of ions against V_G. (b) Transfer characteristics of ion-gated InP at room temperature. The value of I_D under V_G was suppressed in an O_2 gas environment, as in the case of $SrTiO_3$.

B. Ionic gating in an O_2-gas atmosphere

It is important to eliminate possible sources of chemical reactions, e.g., some kind of gas molecules in the ionic liquid [8,18], during the carrier accumulation process in order to evaluate the nature or the ionic gating. In particular, the effect of O_2 gas in ionic liquids should be investigated because it has been reported that I_D in ion-gated $SrTiO_3$ is suppressed under an O_2 gas atmosphere [8]. Before starting the thermoelectric measurements, we performed a control experiment on the transistor operations of $SrTiO_3$ and InP-based ion-gated devices under three different conditions: high vacuum, He, and O_2 atmosphere.

First, we measured the transfer curve (I_D-V_G characteristics) of the ion-gated $SrTiO_3$ (device D). Figure 2(a) shows the transfer characteristics at room temperature for different gas atmospheres. In a high vacuum condition, where the pressure in the sample space is $\sim 10^{-5}$ Torr, a nice n-type transistor operation was observed (black circles). We also monitored the reference voltage V_{Ref} to measure the actual bias voltage applied on the $SrTiO_3$ surface. We prepared a gold pseudoreference electrode, as reported elsewhere [24,25]. The inset of Fig. 2 shows I_D against V_{Ref}, in which the hysteresis of the transfer curve is very tiny. This suggests that the hysteresis in the I_D-V_G characteristics in Fig. 2 originates from the slow reformation of ions against V_G. Then we introduced 10 Torr of He gas into the sample space. The transfer characteristics do not change so much (gray circles). After this, we pumped the He gas in the chamber and introduced a certain amount of high-purity O_2 gas (purity >99.999 95%). In this case, as shown in the figure, I_D was dramatically suppressed upon increasing the O_2 gas pressure from 1 to 100 Torr (red, green, and pink circles). Secondly, we conducted the same experiment on InP single crystal, which is a typical nonoxide semiconductor. Figure 2(b) shows the transfer characteristics of the ion-gated InP; we found the suppression of I_D under an O_2 gas environment, as in the case of $SrTiO_3$.

The suppression of I_D by O_2 gas exposure occurred not only in $SrTiO_3$ but also in InP-based devices. This result indicates that the O_2 gas introduced in the ionic dielectric media would disturb the charge accumulation at the channel regardless of the channel materials, resulting in a poor gate response. It has been widely recognized that the O_2 gas in ionic liquid induces the oxygen reduction reaction on the surface of electrodes [26,27]. Under the application of electric voltage through ionic liquid, an O_2 molecule receives one electron from the electrode and ionizes to form a peroxide ion O_2^{1-}. This process is probably the origin of the suppression of the transfer characteristics shown in Fig. 2. Therefore, in this study, we performed all the experiments in a vacuum condition with a chamber pressure of $\sim 10^{-5}$ Torr in order to avoid the impact of gas molecules on the ion-gated devices.

C. Field-effect control of diffusive thermopower in $SrTiO_3$

Figure 3 shows the variation of the absolute value $|S|$ for the ion-gated device, device E, as a function of sheet carrier density N (lower axis) or volume carrier density n (upper axis) at 200 K. The values of N were estimated using the calibration curve between R_s and N. The values of n were evaluated for the charge accumulation layer with thickness t as $n = N/t$, where we assumed that t was $\sim$10 nm, referring to the analysis of an anisotropic superconducting critical field of ion-gated $SrTiO_3$ [28]. The values of $|S|$ exhibited a roughly linear decrease against a logarithmic increase in n, as observed in other semiconductors [29]. Also plotted is the n dependence of $|S|$ for reduced $SrTiO_3$ ($SrTiO_{3-\delta}$) single crystals [14,16], La-doped $SrTiO_3$ [(Sr,La)TiO_3] single crystals [15], and thin films [11]. Here note that the n dependence of $|S|$ at 200 K in

device E showed a similar trend to that in single crystals and thin films over a wide range of n.

D. Large phonon-drag response in ion-gated $SrTiO_3$

In spite of the excellent consistency of $|S|$ at 200 K, the low-temperature part showed a dramatic contrast between the ion-gated devices and chemically doped single crystals. The temperature dependence of $|S|$ was measured in the four devices (devices E, F, G, and H) in the metallic conduction regime. The main panel and the inset of Fig. 4(a) show the temperature dependence of $|S|$ and R_s for device E, respectively, when N is $\sim 1.7\times10^{14}$ cm^{-2} (or $n \sim 1.7\times10^{20}$ cm^{-3}) at 200 K. Although device E shows a completely metallic transport [see the inset of Fig. 4(a)], a large enhancement of $|S|$ was observed at around 20 K. This large evolution is attributed to the phonon-drag effect [9,14].

It is known that the observed S generally consists of two independent contributions, namely an electron-diffusion part S_d and a phonon-drag thermopower S_p [9], as $S = S_d + S_p$. The first term originates from the built-in electric field that is produced by the redistribution of charge carriers in the presence of a thermal gradient. The second term corresponds to the momentum exchange between charge carriers and phonons, which drags the charge carriers along the thermal gradient and additively enhances the total thermopower at low temperatures.

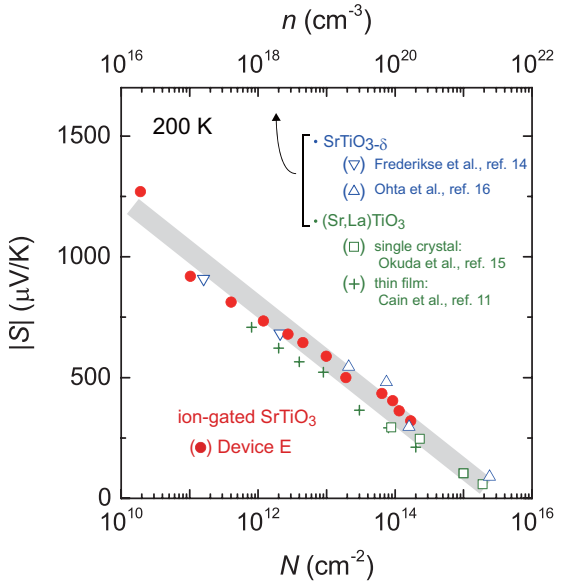

FIG. 3. (Color online) Carrier density dependence of the diffusion Seebeck coefficient in $SrTiO_3$. The Seebeck coefficient S for an ion-gated device (device E) was measured at 200 K in a wide range of carrier density. Here, the absolute value $|S|$ is plotted as a function of sheet carrier density N (lower axis) and volume carrier density n (upper axis). The values of N were estimated from the sheet resistance R_s at 200 K. The values of n are evaluated as $n = N/t$ by assuming that the thickness of the charge accumulation layer t is $\sim$10 nm, referring to the estimation by Ueno *et al.* [4,28]. Also plotted is the n dependence of $|S|$ for the reduced $SrTiO_3$ ($SrTiO_{3-\delta}$) single crystals [14,16], the La-doped $SrTiO_3$ [$(Sr,La)TiO_3$] single crystals [15], and thin films [11]. The n dependence of $|S|$ (at 200 K with a negligible phonon drag effect) in the ion-gated devices shows a fair agreement with that in single crystals and thin films over a wide range of n.

In degenerate semiconductors or metals, the diffusion part is roughly proportional to temperature, and the phonon contribution is negligible at high temperatures (for example at 200 K). The dashed line in Fig. 4(a) depicts the expected diffusion part $|S_d|$ of device E. We find that the phonon-drag contribution dominates the diffusion part at low temperatures. Also plotted are the cases of $SrTiO_{3-\delta}$ single crystal [16] with $n \sim 1.6\times10^{20}$ cm^{-3} and $(Sr,La)TiO_3$ single crystal [15] with $n \sim 2.3\times10^{20}$ cm^{-3}, which have similar values of n with device E. Contrary to the ion-gated device, the phonon-drag effect was totally suppressed in the chemically doped samples, as shown in the figure. Figure 4(b) summarizes the low-temperature peak values of $|S|$ for the ion-gated devices together with the reported data for doped $SrTiO_3$ single crystals [15,16] and thin films [11]. We found that the peak values of $|S|$ in ion-gated devices were much larger than those in chemically doped samples, reflecting the amplitude of $|S_p|$.

IV. DISCUSSION

It is known, in general, that $|S_p|$ is suppressed by the disorder in the crystal structure. This is because phonons are easily scattered by the imperfection of the lattice, and the momentum transfer to electrons is hindered. Therefore, the clear contrast of the low-temperature part of $|S|$ between the ion-gated and chemically doped $SrTiO_3$ in Fig. 4 should originate from the amount of impurities. In the case of $SrTiO_{3-\delta}$ and $(Sr,La)TiO_3$, oxygen vacancies or dopant atoms behave as scatterers of phonons, resulting in the reduction of $|S_p|$. Indeed, the impurity effect of phonon-drag thermopower in $SrTiO_3$ has been systematically investigated in La-doped thin films [11], where the large peak of $|S|$ at $\sim$20 K rapidly decreases with increasing La concentration. On the other hand, the low-temperature thermopower in ion-gated $SrTiO_3$ is very large, suggesting that a less disordered metallic state is realized without additional impurities accompanying the carrier doping process. It has been suggested that the metal-insulator transition in ion-gated $SrTiO_3$ occurs as a result of the formation of oxygen vacancies under the strong electric field [8]. However, the present observations, combined with the control experiment on the O_2 gas exposure in Fig. 2, lead us to conclude that the surface charge carriers in ion-gated $SrTiO_3$ are accumulated predominantly in the electrostatic manner, and the electrochemical mechanism is taking a minor role. In addition, a recent study reported that the ionic gating can dope conduction electrons into the $SrTiO_3$ channel even when a thin boron nitride covers the whole channel surface [30], supporting an electrostatic carrier doping mechanism.

While the ion-gating technique has provided a lot of opportunities to observe novel and interesting physical phenomena and also presented possibilities for future electronic device applications, the mechanism of the carrier accumulation has remained contentious. The formation of electric double layers is an interface phenomenon, and it is difficult to trace the process of the carrier accumulation by simply monitoring electronic properties. Our approach has focused on phonons in the conduction channel and successfully extracted the predominant carrier accumulation mechanism. We may note

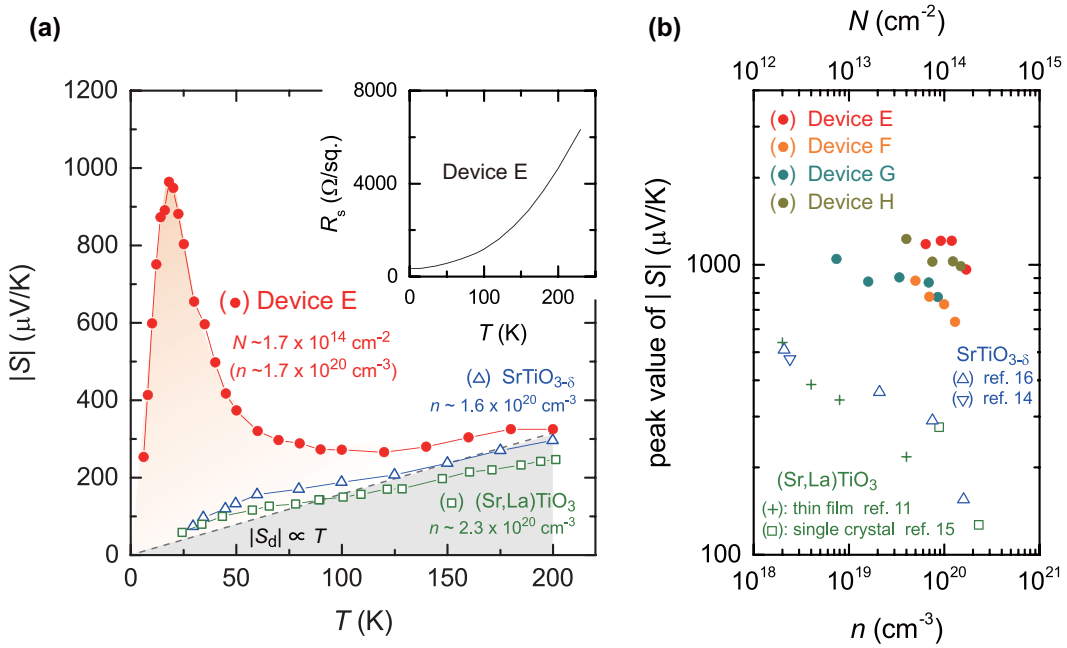

FIG. 4. (Color online) Phonon-drag thermopower in $SrTiO_3$-based ion-gated transistors. (a) Comparison of Seebeck coefficient S between $SrTiO_3$-based ion-gated transistor (device E), reduced $SrTiO_3$ ($SrTiO_{3-\delta}$) single crystal [16], and La-doped $SrTiO_3$ [$(Sr,La)TiO_3$] single crystal [15]. Here, the absolute value $|S|$ is plotted as a function of temperature T. The samples presented here have similar values of n, which is 1×10^{20} to 2×10^{20} cm^{-3}. The dashed line is the rough estimation of the diffusion part $|S_d|$ in device E, assuming that $|S_d|$ is proportional to T and that the phonon contribution is negligible at 200 K. The large peak in $|S|$ at low temperatures is attributed to the phonon-drag effect. The inset figure presents the T dependence of the sheet resistance R_s in device E, which shows the metallic conduction behavior. (b) Low-temperature peak values of $|S|$ as a function of n (lower axis) or N (upper axis) for ion-gated $SrTiO_3$ (devices E, F, G, and H) and chemically doped $SrTiO_3$ [11,14–16]. These low-temperature peaks are dramatically enhanced in ion-gated devices.

here that the large S_p with the metallic charge transport in ion-gated $SrTiO_3$ is similar to the cases in two-dimensional systems realized at semiconductor heterointerfaces [31–34]. The charge carriers are confined in disorder-free conduction layers by modulation doping, and they demonstrate large S_p due to the interaction with phonons that have large λ.

The field-induced and chemically doped metallic states are schematically illustrated in Figs. 5(a) and 5(b), respectively, where electrons and phonons travel along the thermal gradient $-\nabla T$. In the case of the ion-gated $SrTiO_3$, λ is expected to be very large at low temperatures because λ is proportional to $|S_p|$. According to the kinetic theory, λ at 20 K is estimated to be several hundred nanometers, which is comparable to that in pure $SrTiO_3$ single crystal (see the Appendix). On the other hand, λ should be suppressed in chemically doped metallic $SrTiO_3$, as sketched in Fig. 5(b). The value of λ is found to be several tens of nanometers, which was reduced to one order of magnitude smaller than that in pure $SrTiO_3$. This striking difference of the phonon states is highlighted in the power factor, which is defined from S and the electrical conductivity σ as $S^2\sigma$. Figure 5(c) compares the power factor $(S^2\sigma)_{2D}$ for the ion-gated $SrTiO_3$ and $(S^2\sigma)_{3D}$ for a $(Sr,La)TiO_3$ thin film [11] both with $n \sim 2\times10^{20}$ cm^{-3}. Here, the values of σ for the ion-gated $SrTiO_3$ were estimated as $\sigma = 1/(R_s t)$, assuming $t \sim 10$ nm as discussed above. It should be noted that the power factor in the ion-gated $SrTiO_3$ is two orders of magnitude larger than that in the $(Sr,La)TiO_3$ thin film at around the peak temperature (~20 K). Indeed, the peak values of the power factor are larger than any reported values in chemically doped bulk $SrTiO_3$ and furthermore are comparable to the highest recorded value in $FeSb_2$ [35]. The large λ, which is realized in

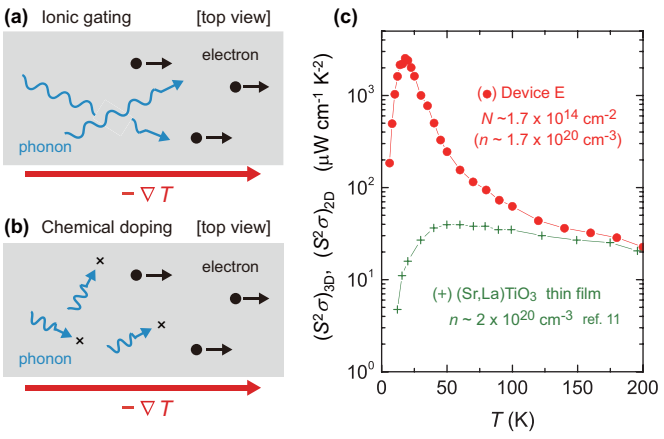

FIG. 5. (Color online) Enhancement of power factor in ion-gated $SrTiO_3$. (a),(b) Schematic top-view illustration of phonon states at low temperatures under the thermal gradient $-\nabla T$. Field-effect doping and chemical doping correspond to (a) and (b), respectively. The phonon mean free path becomes very large at low temperatures in (a) but is totally suppressed due to the impurity in (b). (c) Comparison of power factor, $S^2\sigma$, for ion-gated $SrTiO_3$ (this work) and $(Sr,La)TiO_3$ thin film [11] both with $n \sim 2\times10^{20}$ cm^{-3}. Here, S and σ are the Seebeck coefficient and conductivity, respectively. The power factor in ion-gated $SrTiO_3$ is two orders larger than that in the $(Sr,La)TiO_3$ thin film at around the peak temperature (~20 K).

TABLE I. Phonon mean free path λ at 20 K in nondoped $SrTiO_3$ and Nb-doped $SrTiO_3$ [Sr(Ti,Nb)O_3] with 3% Nb doping. The volume carrier density n for Sr(Ti,Nb)O_3 is 5.48×10^{20} cm^{-3}. The values of λ were estimated by using Eq. (A1) and the literature values in this table. Here, κ_p, C_p, and ν are the lattice thermal conductivity, the lattice specific-heat capacity, and the averaged sound velocity, respectively, at 20 K.

	λ (nm)	n (10^{20} cm^{-3})	κ_p (W K^{-1} m^{-1})	C_p (J K^{-1} mol^{-1})	ν (m s^{-1})
Nondoped $SrTiO_3$	~740	N/A	~20 [37]	~0.57 [38]	~5400 [39]
Sr(Ti,Nb)O_3	~24	~5.48 [17]	~20 [17]	~0.57 [17]	~5400 [39]

electrostatically induced metallic states, greatly enhances the cryogenic thermoelectric responses in the ion-gated $SrTiO_3$.

V. SUMMARY

In summary, we have demonstrated the enhancement of the cryogenic thermopower in the ion-gated $SrTiO_3$. The Seebeck coefficient increased with decreasing temperature due to the development of the phonon mean free path and reached as large as 1 mV/K at 20 K. Through the comparison between the chemically doped bulk $SrTiO_3$ and the ion-gated $SrTiO_3$, we found that the chemical carrier doping, such as La doping and oxygen deficiency, totally suppressed the phonon-drag contribution due to the chemical disorder, while the ionic gating sustained the large phonon-drag peak even in a metallic regime with a carrier density as large as 2×10^{14} cm^{-2}. In addition, the thermoelectric power factor also clearly reflected the difference of the carrier doping process, showing that the power factor in the ion-gated $SrTiO_3$ is about two orders of magnitude larger than that of chemically doped $SrTiO_3$. These experimental results suggest that the electrostatic carrier doping is predominantly realized in the carrier doping process in the ion-gated $SrTiO_3$.

ACKNOWLEDGMENTS

We are grateful to T. Suzuki, A. Kikkawa, and S. Shimano for their fruitful discussions and technical support. This work was supported by the Strategic International Collaborative Research Program (SICORP-LEMSUPER), the Japan Science and Technology Agency (JST), JSPS Grant-in-Aid for Scientific Research (S) (No. 24224009), JSPS Grant-in-Aid for Specially Promoted Research (No. 25000003), JSPS Grant-in-Aid for Scientific Research (B) (No. 26288115), JSPS Grant-in-Aid for Young Scientist (B) (No. 26820298), and JSPS Grant-in-Aid for Young Scientist (B) (No. 26790052).

APPENDIX: ESTIMATION OF THE PHONON MEAN FREE PATH

The phonon mean free path λ is sensitive to the defect or dopant density in the crystal structure. According to kinetic theory [36], the lattice thermal conductivity κ_p is expressed by

$$\kappa_p = C_p \nu \lambda / 3, \tag{A1}$$

where C_p is the phonon contribution to the total specific-heat capacity, and ν is the sound velocity. From literature values of κ_p [17,37], C_p [17,38], and ν [39], we estimated λ for nondoped $SrTiO_3$ and Nb-doped $SrTiO_3$ [Sr(Ti,Nb)O_3] single crystals at 20 K, as listed in Table I. We found that λ for Sr(Ti,Nb)O_3 with 3% Nb doping was drastically suppressed compared to that for nondoped $SrTiO_3$.

It is known that λ is proportional to the phonon-drag thermopower S_p [9,10]. Although it is difficult to precisely deduce S_p from the total thermopower S, the magnitude of S_p in the ion-gated $SrTiO_3$ would be 10 to 20 times larger than that in the chemically doped $SrTiO_3$ at 20 K in Fig. 4(a). Therefore, λ in the ion-gated $SrTiO_3$ (device E) with $n \sim 1.7\times10^{20}$ cm^{-3} is roughly estimated to be 240 to 480 nm, assuming that λ in the chemically doped $SrTiO_3$ discussed in Fig. 4(a) is comparable to that of Sr(Ti,Nb)O_3 with 3% Nb doping. Surprisingly, λ in the ion-gated $SrTiO_3$ is not as reduced from that in nondoped $SrTiO_3$; this reflects the less disordered nature of the carrier accumulation process in the ionic gating.

[1] M. Nakano, K. Shibuya, D. Okuyama, T. Hatano, S. Ono, M. Kawasaki, Y. Iwasa, and Y. Tokura, Nature (London) **487**, 459 (2012).
[2] J. Jeong, N. Aetukuri, T. Graf, T. D. Schladt, M. G. Samant, and S. S. P. Parkin, Science **339**, 1402 (2013).
[3] Y. Yamada, K. Ueno, T. Fukumura, H. T. Yuan, H. Shimotani, Y. Iwasa, L. Gu, S. Tsukimoto, Y. Ikuhara, and M. Kawasaki, Science **332**, 1065 (2011).
[4] K. Ueno, S. Nakamura, H. Shimotani, A. Ohtomo, N. Kimura, T. Nojima, H. Aoki, Y. Iwasa, and M. Kawasaki, Nat. Mater. **7**, 855 (2008).
[5] A. T. Bollinger, G. Dubuis, J. Yoon, D. Pavuna, J. Misewich, and I. Božović, Nature (London) **472**, 458 (2011).
[6] X. Leng, J. Garcia-Barriocanal, S. Bose, Y. Lee, and A. M. Goldman, Phys. Rev. Lett. **107**, 027001 (2011).
[7] J. T. Ye, Y. J. Zhang, R. Akashi, M. S. Bahramy, R. Arita, and Y. Iwasa, Science **338**, 1193 (2012).
[8] M. Li, W. Han, X. Jiang, J. Jeong, M. G. Samant, and S. S. P. Parkin, Nano Lett. **13**, 4675 (2013).
[9] C. Herring, Phys. Rev. **96**, 1163 (1954).
[10] L. Weber and E. Gmelin, Appl. Phys. A **53**, 136 (1991).
[11] T. A. Cain, A. P. Kajdos, and S. Stemmer, Appl. Phys. Lett. **102**, 182101 (2013).
[12] J. P. Issi and J. Boxus, Cryogenics (Guildf). **19**, 517 (1979).
[13] S. R. Harutyunyan, V. H. Vardanyan, A. S. Kuzanyan, V. R. Nikoghosyan, S. Kunii, K. S. Wood, and A. M. Gulian, Appl. Phys. Lett. **83**, 2142 (2003).
[14] H. P. R. Frederikse, W. R. Thurber, and W. R. Hosler, Phys. Rev. **134**, A442 (1964).

[15] T. Okuda, K. Nakanishi, S. Miyasaka, and Y. Tokura, Phys. Rev. B **63**, 113104 (2001).
[16] H. Ohta, S. Kim, Y. Mune, T. Mizoguchi, K. Nomura, S. Ohta, T. Nomura, Y. Nakanishi, Y. Ikuhara, M. Hirano, H. Hosono, and K. Koumoto, Nat. Mater. **6**, 129 (2007).
[17] J. Fukuyado, K. Narikiyo, M. Akaki, H. Kuwahara, and T. Okuda, Phys. Rev. B **85**, 075112 (2012).
[18] H. Yuan, H. Shimotani, A. Tsukazaki, A. Ohtomo, M. Kawasaki, and Y. Iwasa, J. Am. Chem. Soc. **132**, 6672 (2010).
[19] D. W. Reagor and V. Y. Butko, Nat. Mater. **4**, 593 (2005).
[20] M. A. B. H. Susan, T. Kaneko, A. Noda, and M. Watanabe, J. Am. Chem. Soc. **127**, 4976 (2005).
[21] J. Lee, M. J. Panzer, Y. He, T. P. Lodge, and C. D. Frisbie, J. Am. Chem. Soc. **129**, 4532 (2007).
[22] H. Ohta, Y. Masuoka, R. Asahi, T. Kato, Y. Ikuhara, K. Nomura, and H. Hosono, Appl. Phys. Lett. **95**, 113505 (2009).
[23] Y. Lee, C. Clement, J. Hellerstedt, J. Kinney, L. Kinnischtzke, X. Leng, S. D. Snyder, and A. M. Goldman, Phys. Rev. Lett. **106**, 136809 (2011).
[24] D. Braga, I. Gutiérrez Lezama, H. Berger, and A. F. Morpurgo, Nano Lett. **12**, 5218 (2012).
[25] Y. Xia, J. Cho, B. Paulsen, C. D. Frisbie, and M. J. Renn, Appl. Phys. Lett. **94**, 013304 (2009).
[26] Y. Katayama, H. Onodera, M. Yamagata, and T. Miura, J. Electrochem. Soc. **151**, A59 (2004).
[27] E. E. Switzer, R. Zeller, Q. Chen, K. Sieradzki, D. A. Buttry, and C. Friesen, J. Phys. Chem. C **117**, 8683 (2013).
[28] K. Ueno, T. Nojima, S. Yonezawa, M. Kawasaki, Y. Iwasa, and Y. Maeno, Phys. Rev. B **89**, 020508(R) (2014).
[29] D. M. Rowe and G. Min, J. Mater. Sci. Lett. **14**, 617 (1995).
[30] P. Gallagher, M. Lee, T. A. Petach, S. W. Stanwyck, J. R. Williams, K. Watanabe, T. Taniguchi, and D. Goldhaber-Gordon, Nat. Commun. **6**, 6437 (2015).
[31] R. Fletcher, M. D'Iorio, A. S. Sachrajda, R. Stoner, C. T. Foxon, and J. J. Harris, Phys. Rev. B **37**, 3137 (1988).
[32] B. L. Gallagher, J. P. Oxley, T. Galloway, M. J. Smith, and P. N. Butcher, J. Phys.: Condens. Matter **2**, 755 (1990).
[33] S. Agan, O. A. Mironov, E. H. C. Parker, and T. E. Whall, Semicond. Sci. Technol. **15**, 551 (2000).
[34] I. Pallecchi, F. Telesio, D. Li, A. Fête, S. Gariglio, J.-M. Triscone, A. Filippetti, P. Delugas, V. Fiorentini, and D. Marré, Nat. Commun. **6**, 6678 (2015).
[35] A. Bentien, S. Johnsen, G. K. H. Madsen, B. B. Iversen, and F. Steglich, Europhys. Lett. **80**, 17008 (2007).
[36] J. M. Jiman, *Electrons and Phonons* (Oxford University Press, Oxford, 1967).
[37] Y. Suemune, J. Phys. Soc. Jpn. **20**, 174 (1965).
[38] M. Ahrens, R. Merkle, B. Rahmati, and J. Maier, Physica B **393**, 239 (2007).
[39] R. Bell and G. Rupprecht, Phys. Rev. **129**, 90 (1963).